Mode-Coupling Generation by ITO Nanodisk Arrays With Au Substrate Enabling Narrow-Band Biosensing

Shuwen Chu , Yuzhang Liang , Mengdi Lu , Huizhen Yuan , Yi Han , Jean-Francois Masson , Wei Peng *

Posted Date: 10 May 2023

doi: 10.20944/preprints202305.0721.v1

Keywords: ITO nanodisk; nanostructure; coupling mode; biosensing; narrow band

Article

Mode-Coupling Generation by ITO Nanodisk Arrays with Au Substrate Enabling Narrow-Band Biosensing

Shuwen Chu [1], Yuzhang Liang [1], Mengdi Lu [1], Huizhen Yuan [1], Yi Han [2], Jean-Francois Masson [3] and Wei Peng [1,*]

[1] School of Physics, Dalian University of Technology, Dalian, 116024, China; Chuswdlut@163.com (S.C.); yzliang@dlut.edu.cn (Y.L.); mdlu@dlut.edu.cn (M.L.); hzyuan@dlut.edu.cn (H.Y.)

[2] Department of Anaesthesia, Second Hospital of Shanxi Medical University, Taiyuan 030001, Shanxi, China; 13753171979@163.com

[3] Département de Chimie, Regroupement Québécois des Matériaux de Pointe, and Centre Québécois sur les Matériaux Fonctionnels (CQMF), Université de Montréal, Montreal, QC H3C 3J7, Canada; jf.masson@umontreal.ca

* Correspondence: wpeng@dlut.edu.cn

Abstract: Metal plasmonic nanostructures have promising applications in biosensing due to their ability to facilitate light-matter interaction. However, the damping of the metal leads to a wide full width at half maximum (FWHM) spectrum and results which restricts its sensing capabilities. In this research, we present a novel non-full-metal nanostructure, namely indium-tin oxide (ITO)-Au nanodisk arrays consisting of top ITO nanodisk arrays and a bottom gold layer, and compare the coupling mode with the full-metal nanodisk arrays. The FWHM of proposed ITO-Au nanodisk array reduces to one fifth of that all metal nanodisk arrays, which is generated mode-coupling by surface plasmon modes at metal interfaces with magnetic resonance mode. Furthermore, the thickness variation of nanodisks has no impact on the sensing performance of this ITO-based nanostructure, ensuring excellent tolerance during preparation. We fabricated both structures by using template transfer and vacuum deposition techniques and calibrated their sensing performances by detect Immunoglobulin G (IgG) protein molecules. Both theoretical and experimental results demonstrate that ITO-Au nanodisk arrays provide an effective solution for biosensing applications.

Keywords: ITO nanodisk; nanostructure; coupling mode; biosensing; narrow band

1. Introduction

Surface plasmon polaritons (SPPs) possess subwavelength confinement of light and breakthrough diffraction limits, which has obtained significantly progresses in color filter [1,2], perfect absorber [3–5], nano laser [6,7], and chemical or biosensor [8,9]. The coherent oscillations of free electrons at the surface of metal are extremely sensitive to refractive index (RI) changes of the surrounding medium, which enables plasmonic sensors to detect molecular interactions in fast, real-time, and free-label. Traditional plasmonic sensors relay on propagating SPPs excited by the prism coupling or local localized surface plasmon resonance (LSPR) excited nanoparticles and nanostructures. Compared to the excitation of prism coupling requiring large and accurate optical devices, metal nanostructures are powerful platform for the rapid development of multichannel and point of care testing (POCT) technology. Nevertheless, the inherent dispersion loss of metal materials in the visible region results in a wider full width at half maximum (FWHM), which immensely restrict the development of nanostructure biosensing [10–12]. In order to promote the sensing performance, hybridization coupling of different resonant modes or introducing compound materials can gain narrower bandwidth and higher sensitivity [13–15].

Preprints (www.preprints.org) | NOT PEER-REVIEWED | Posted: 10 May 2023 doi:10.20944/preprints202305.0721.v1

Various strategies have been employed in fabrication of the nanostructure arrays, involving two steps: template fabrication and film deposition. The most commonly preparing nanostructures technology mainly include electron-beam lithography (EBL), focused-ion-beam lithography (FIB), nanosphere lithography, nanoimprint lithography, and anodic aluminum oxide (AAO) template-based lithography [16,17]. An ideal nanofabrication technique would be inexpensive, high throughput, high resolution, and provides great flexibility for customizing the size and shape of nanostructure. Wherein, AAO template-based lithography is undoubtedly the best choice for achieving large area and low-cost nanostructures [18].

Herein, we proposed an ultra-narrow band sensor featuring indium-tin oxide (ITO) nanodisk arrays coupled with metal substrate. The plasmonic structure is numerically modeled using finite difference time domain (FDTD) method, to investigate the effect of various design parameters on the sensing performance. In this architecture, the interaction between ITO nanodisks and Au substrates leads to the excitation of lattice mode and SPP mode, resulting in a bandwidth of only 14 nm. This value is one fifth that obtained with gold nanodisk arrays of the same period. What's exciting is that changing the height of disks hardly affects the sensing figure of merit (FOM), which improves the process tolerance for the preparation. The large-area nanostructures are fabricated through template transfer and magnetron sputtering coating. The potential for biosensing has been demonstrated using molecular specific recognition.

2. Results and Discussion

Our proposed ultra-narrow band biosensor and typical spectrum are shown in Figure 1. Figure 1a illustrates the schematic and geometric parameters of our proposed structure. ITO nanodisks arranged in hexagonal arrays are integrated on gold substrate, namely ITO-Au nanodisk arrays. The period of unit cell is P=450 nm. The diameter and thickness of the nanodisk are D=360 nm and t, respectively. The thickness of the gold substrate is fixed at 100 nm, which provides the function of a mirror. The TM polarization light is incident along the z-direction. Numerical simulation with a finite-difference time-domain (FDTD) algorithm is performed to obtain reflection spectra and field distributions around resonance dips. In the simulations, periodic boundary conditions are used along the x and y directions, and perfectly matched layers are used in the z direction. The grid size along the x, y, and z directions is 1 nm×3.46 nm×2 nm, respectively. The permittivity of Au and ITO in the visible and near-infrared region is obtained from experimental results. We obtained the refractive index (n) and extinction coefficient (k) of the material using Ellipsometry, as shown in Figure 2a. The refractive index of silica substrate is 1.46.

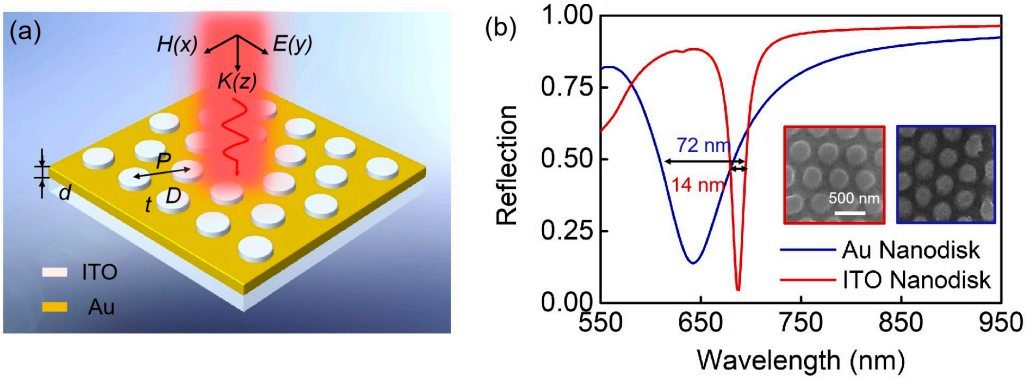

Figure 1. Ultra-narrow band biosensor. (a) Schematic diagram of ITO-Au nanodisk arrays. (b) Simulated reflection spectra and SEM images of the two nanostructures. The red line and block diagram represent ITO-Au nanodisk arrays, and the blue ones indicate full-metal nanodisk arrays.

To illustrate the advantages of our proposed structure, we have compared it with Au nanodisk arrays on the Au substrate assuming full-metal nanostructures. Figure 1b depicts the calculated

Preprints (www.preprints.org) | NOT PEER-REVIEWED | Posted: 10 May 2023 doi:10.20944/preprints202305.0721.v1

spectra of reflection for the patterned Au nanodisk and ITO nanodisk integrated with Au layer when the refractive index of cover layer is n=1.3313. Our proposed ITO-Au nanodisk arrays reduces the FWHM down to 14 nm, leading to an ultra-narrow band resonance mode. Significantly, the FWHM of full-metal nanodisk arrays is five times that of it. In order to reveal the optical properties and sensing applications of proposed structure, we conducted comparative analysis of the ITO-Au nanodisk arrays and full-metal nanodisk arrays. The insets show the experimentally obtained structure with highly ordered hexagonal array of nanodisks.

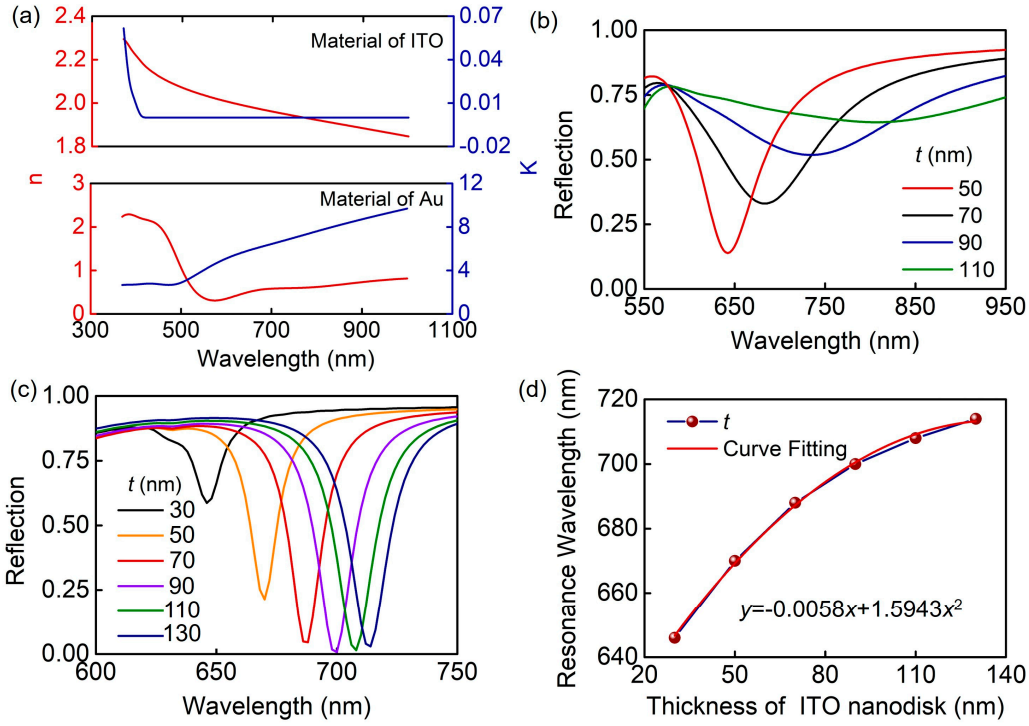

Figure 2. Optical properties of ITO-Au nanodisk arrays and full-metal nanodisk arrays under normal incidence. (a) The refractive index (n) and extinction coefficient (k) of the material for ITO and Au using Ellipsometry. (b) Spectral shift as the thickness of Au nanodisks (t). (c) Spectral shift and (d) resonance wavelength as the thickness of ITO nanodisks (t).

Figure 2 illustrates the simulation results for both two nanodisk arrays. When the other structural parameters are fixed, the thickness (t) of nanodisks has different effects on the reflection spectra of the two structures. As shown in Figure 2b,c, with an increase in thickness, the resonance wavelength shifts to the red side for both structures. Nevertheless, the reflection depth decreases sharply, accompanied by a significant broadening of FWHM for all-metal nanodisk arrays. In contrast, the reflection depth of ITO-Au nanodisk arrays gradually increases. When it reaches 70 nm, the resonance intensity hardly changes. In this condition, the wavelength dependency of the thinkness of nanodisk-can be disregarded. In addition, the relationship between thickness and resonance wavelength is established using polynomial fitting, as shown in Figure 2d. Therefore, flexible regulation of the resonance wavelength position can be achieved by controlling the thickness of the nanodisk.

To explain the different modes of two structures, Figure 3 maps the distribution of electric field in the xy-plane and xz-plane at 648 nm and 684 nm, respectively. The fields are normalized to the field amplitude of the incident light (E/E_0). Wherein, white dashed boxes indicate metal material, while blue ones indicate ITO material. As shown in Figure 3a,b, the energy is localized at the edge of the Au-nanodisks. And the inset is the variation of electric field intensity along the z direction of orange dotted line. The opaque gold film hinders the transmission of incident light to the silica substrate and forms coupling modes based on the film and Au nanodisk arrays. The diffraction coupling of local dipole modes leads to the excitation of surface plasmon Bloch mode [19]. For ITO-

Preprints (www.preprints.org) | NOT PEER-REVIEWED | Posted: 10 May 2023 doi:10.20944/preprints202305.0721.v1

Au nanodisk arrays, the electric field is mainly localized at the interfaces between the disks and the Au layer, and the disks and measuring solution (Figure 3c). The near-field intensity decreases exponentially, which is consistent with the characteristics of propagating surface plasmon mode for infinite planar noble film. The generation of dipolar plasmon mode originates from lattice resonance of the hexagonal ITO nanodisk diffraction field. In addition, the narrow band excitation in this structure is also attributed to magnetic resonance that combines the magnetic field distribution, i.e., strong magnetic field distribution in the ITO nanodisks, and the charge distribution on the upper and underneath surfaces of the disks. Therefore, the narrow-band resonance is the coupling of propagating surface plasmon mode resonances on the upper and bottom surfaces of the gold film with magnetic resonance of nanodisk arrays. This explains that changes in the height of disks can affect the resonance wavelength. The results indicate that the introduction of ITO nanodisks effectively reduces the inherent loss of metal materials. Unfortunately, most of the excited electric field is hidden beneath nanodisks, which is unfavorable for biosensing.

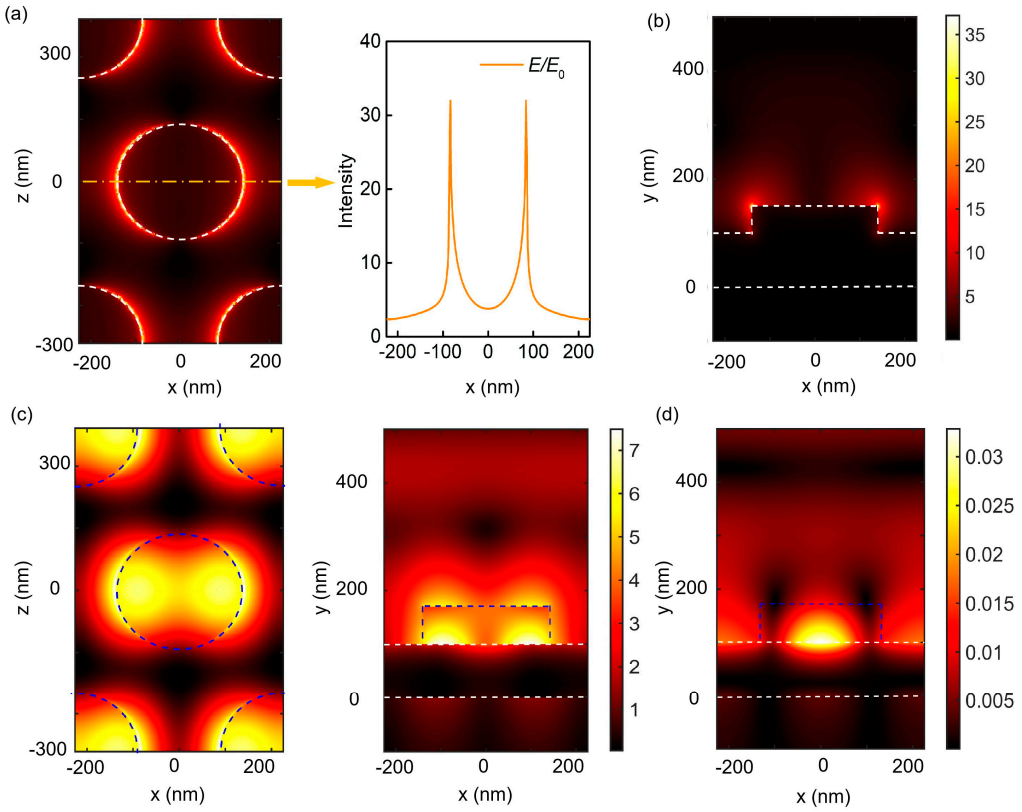

Figure 3. Electromagnetic field distribution of resonance wavelengths for two structures. The field is normalized to the field amplitude of the incident light (E/E_0) and corresponding magnetic field distribution. Electric field distributions at (a) *xy* plane, and (b) *xz* plane for *y*=150 nm for full-metal nanodisk array. Inset is the variation of electric field intensity along the *z* direction of orange dotted line. (c) Electric field distributions of *xy* plane and *xz* plane with *y*=170 nm, and (d) magnetic field distribution of *xz* plane with *y*=170 nm for ITO-Au nanodisk arrays. White dashed line indicate metal material, while blue dashed line indicates ITO material.

In order to evaluate the overall performance of the proposed coupling sensors, we adopt the widely used sensitivity and bulk FOM. Wherein, sensitivity (S) can be defined as the amount of wavelength shift $\Delta\lambda$ as a function of the induced RI change [20,21]:

$$S = \frac{\Delta\lambda}{\Delta n} \tag{1}$$

And the FOM depends on the ratio of sensitivity *S* and FWHM [21,22]:

Preprints (www.preprints.org) | NOT PEER-REVIEWED | Posted: 10 May 2023 doi:10.20944/preprints202305.0721.v1

$$\mathrm{FOM} = \frac{S}{\mathrm{FWHM}} \tag{2}$$

It is worth mentioning that the definition of S here refers to bulk sensitivity.

As shown in Figure 4, we have calculated the reflection of proposed structure with a cover layer for different refractive indices. For the full-metal nanodisk arrays, the position of the dip redshifts from 650 nm to 675 nm when the refractive index increases from 1.33 to 1.38 (Figure 4a), while the value of reflective dip and the lineshape of resonance remains constant. Figure 4b extracts the positions of reflection dip from Figure 4a to plot them as a function of refractive indices and represents the blue line as the line fitting. The slope of resonance mode is 480 nm/RIU and the bulk FOM is 6.67. For the ITO-Au nanodisk arrays, the resonance dip redshifts from 684 nm to 695 nm when the refractive index changes from 1.33 to 1.38, as illustrated in Figure 4c. The slope of plasmonic resonance is 200 nm/RIU and the bulk FOM is 14.28 when the thickness is 70 nm, which is twice as comparable to the sensitivity of full-metal nanodisk arrays. Furthermore, we discuss the changes in sensitivity and FOM under different thicknesses. The results declare the values remain unchanged in the range of 70-90 nm, which greatly improves the tolerance of preparation process for our proposed structure (Figure 4d).

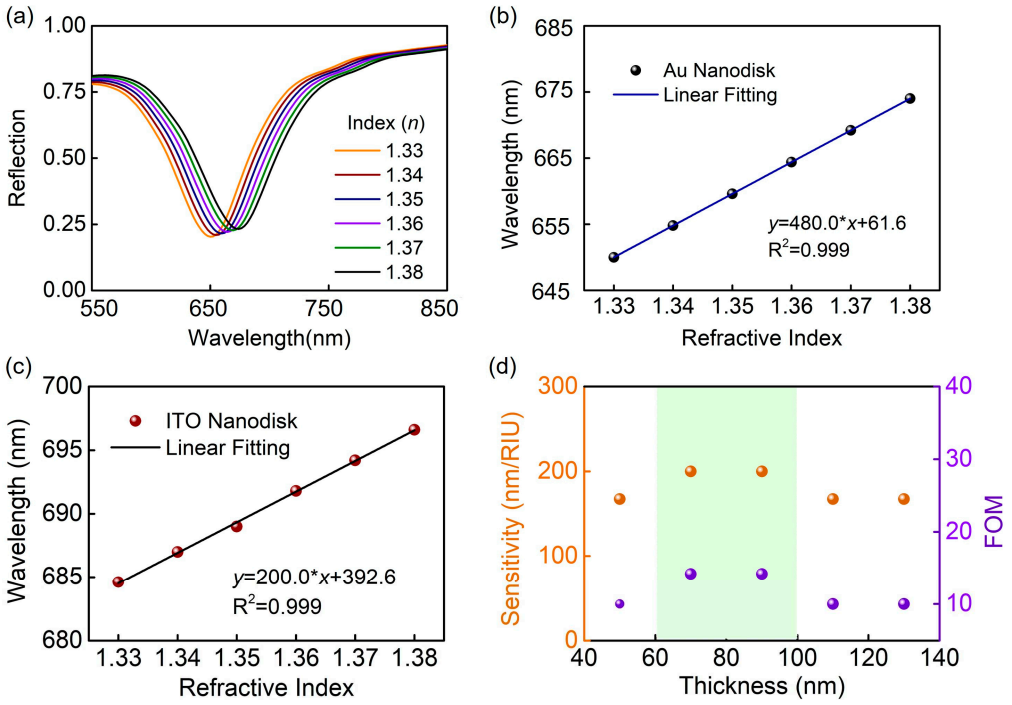

Figure 4. Calculated reflection of full-metal nanodisk arrays and ITO-Au nanodisk arrays with different values of refractive index on the surface. (a) Reflection spectra and (b) resonance wavelengths as functions of RI with the cover layer for full-metal nanodisk arrays. (c) Resonance wavelengths as a functions of RI and (d) the influence of different thicknesses on refractive index sensitivity and FOM for ITO-Au nanodisk arrays.

In essence, bulk sensitivity describes the measurement of accessible field regions from the surface of nanostructure sensors to infinity. Nevertheless, it is inappropriate for biological molecules, such as proteins, DNA, and viruses. In order to more accurately judge the performance of sensor response, the surface sensitivity is used for evaluation. It describes the change caused by the refractive index of thin layer near the sensor surface. To quantify the performance of sensors, a molecular layer with a refractive index of 1.45 is covered on the surface. We investigate the spectra of reflection with varying thicknesses. Obviously, the resonance wavelengths of both structures undergo redshift as the thickness of the protein layer increases from 0 to 30 nm. The dependence of resonance wavelength

Preprints (www.preprints.org) | NOT PEER-REVIEWED | Posted: 10 May 2023 doi:10.20944/preprints202305.0721.v1

on the distance from surface is considered, so we fit the data in Figure 5a to exponential curves. The formula is as follows [23,24]:

$$\Delta\lambda = \Delta\lambda_{\infty}(1-e^{-d/l_d}) \tag{3}$$

Wherein $\Delta\lambda_{\infty}$ denotes the wavelength shift induced by a layer with an infinite thickness. d is the thickness of additional layer assuming molecular layer, and ld is related to decay length of electromagnetic field. As shown in Table 1, we obtained $\Delta\lambda_{\infty}$= 119.8 nm and l_d= 48.0 nm^{-1} for all-metal nanodisk arrays and $\Delta\lambda_{\infty}$=54.8 nm and l_d=66.2 nm^{-1} for ITO nanodisk arrays. This further verifies that both structures can achieve sensing applications.

The surface sensitivity is defined as the second derivative of the index and thickness of the adsorbate [25,26]:

$$S_{surf} = \frac{\partial^2\lambda}{\partial d\partial\Delta n} = \frac{\partial\Delta\lambda_{\infty}}{\partial\Delta n}\frac{\partial(1-e^{-d/l_d})}{\partial d} = \frac{\Delta\lambda_{\infty}}{\Delta n l_d}e^{-d/l_d} \tag{4}$$

where Δn= n_{alum}-n_{water}=1.56-1.33=0.23 is the refractive-index change. Figure 5b shows the dependence of surface sensitivity for both resonance modes of two nanostructures on the distance from the structure surface. For ITO-Au nanostructure, partial near-filed enhancement is leaked into the surface of metal substrate, which results in lower sensing performance of surface sensitivity compared to full-metal nanostructure.

Table 1. The comparison of surface sensitivity for the two structures.

	$\Delta\lambda_{\infty}$	l_d
Full-metal nanodisk arrays	119.8 nm	48.0 nm
ITO nanodisk arrays	54.8 nm	66.2 nm

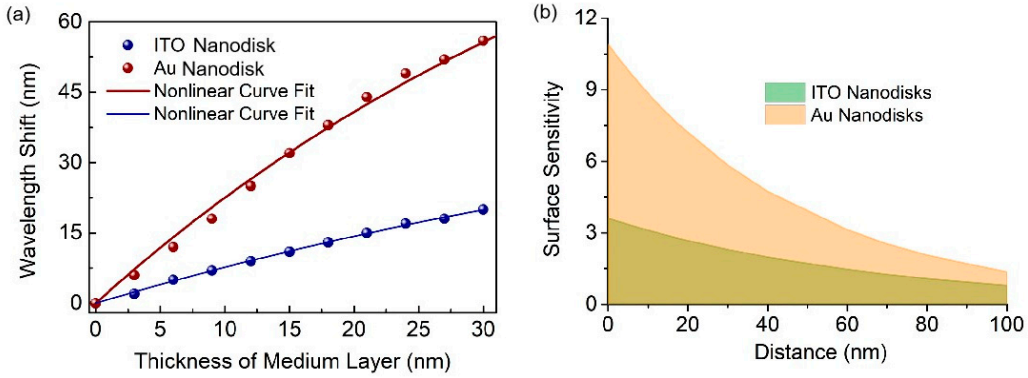

Figure 5. Simulation results of surface sensitivity for the two nanostructures. (a) Resonance wavelength shifts with varied thickness of cover layer. (b) The 2nd order surface sensitivity curve as a function of the adsorbate thickness.

To experimentally investigate the sensitivity of our proposed nanostructure arrays on Au substrate, we utilized template transfer and magnetron sputtering fabrication scheme as illustrated in Figure 6. Firstly, the silicon wafers were cleaned with deionized water, ethanol and acetone under ultrasonic conditions, and then dried with nitrogen. Next, a 100 nm thick gold film was deposited on the surface by magnetron sputtering. An AAO membrane was transferred onto the upper surface of the gold film to serve as a mask. Afterwards, ITO film was deposited on the AAO membrane by sputtering, and finally, the excessive structure was removed, leaving behind ITO nanodisks and a gold film structure. Noting that the AAO template has good periodicity, and the diameter of the nanodisk varied between 260 and 360 nm, which is consistent throughout the preparation of all-metal

Preprints (www.preprints.org) | NOT PEER-REVIEWED | Posted: 10 May 2023 doi:10.20944/preprints202305.0721.v1

nanodisk arrays with the only difference being the second deposition of metal film. The AFM images of the two arrays are shown in the insets of Figure 6a, while the white line profile across the patterns is shown in Figure 6b, which indicates the thickness of the nanodisks in the two structures prepared (i.e., 50 nm for gold nanodisks and 70 nm for ITO).

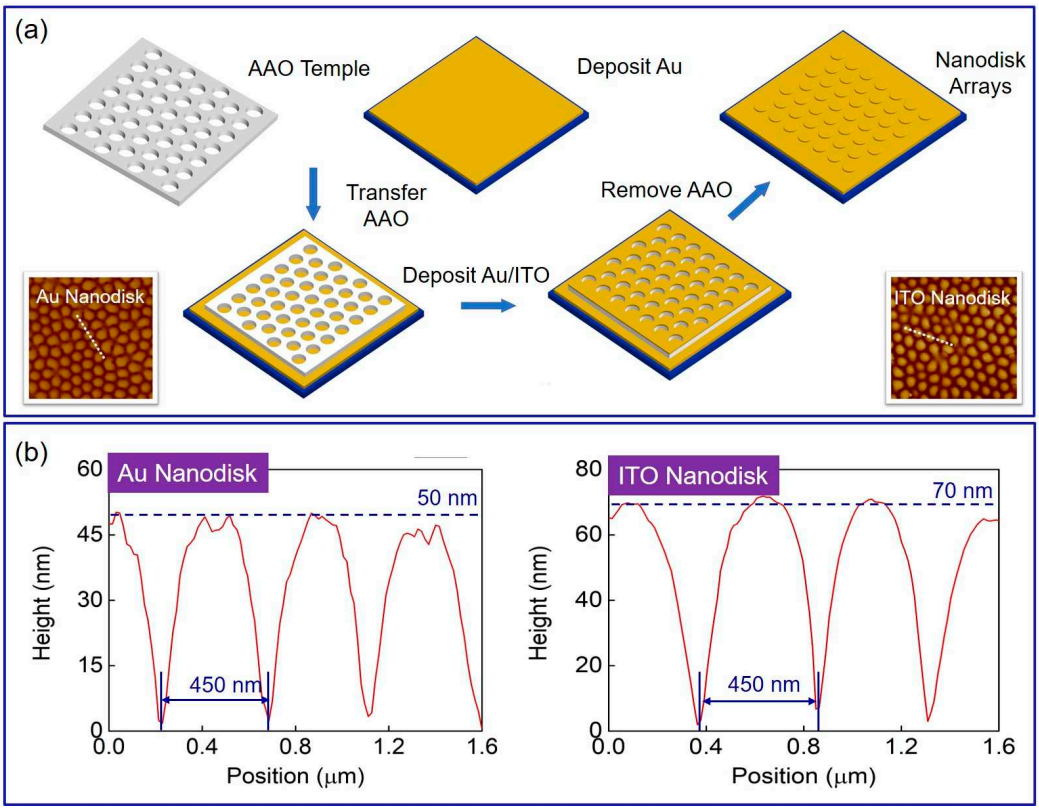

Figure 6. The fabrication of the nanodisk-based structures and AFM image. (a) Scheme for producing low-cost nanodisk structure using template transfer. Insets show AFM images of full-metal nanodisk arrays and ITO-Au nanodisk arrays. (b) The white line profile across the patterns are shown.

Using a home-built reflective spectral detection system, including light source, spectrometer and LabVIEW program, to achieve sensing detection and data acquisition. In Figure 7, the reflection spectra and wavelength response of two structures are shown under normal incidence. Figure 7a,b reveal that the resonance wavelength and FWHM are 660 nm with 69.4 nm and 712 nm with 48.5 nm, respectively. However, the bandwidth is notably wider compared to the simulation results due to the experiment's template quality. The sensitivity has been evaluated by changing the refractive index of measured salt solution analytes, which have been measured using an Abbe refractometer. The prepared structures have been immersed in different concentrations of sodium chloride salt solutions with refractive indices ranging from 1.3314 to 1.3759. As the refractive index increases, the position of the resonance wavelength experiences a redshift, as displayed in Figure 7c,d. The relationship between refractive index and resonant wavelength assumes linear fitting, as demonstrated in Figure 7e,f. And the sensitivity of all-metal nanodisk arrays is S_{Au}=396.0 nm/RIU, while the one of ITO-Au nanodisk arrays is S_{ITO}=193.0 nm/RIU.

Preprints (www.preprints.org) | NOT PEER-REVIEWED | Posted: 10 May 2023 doi:10.20944/preprints202305.0721.v1

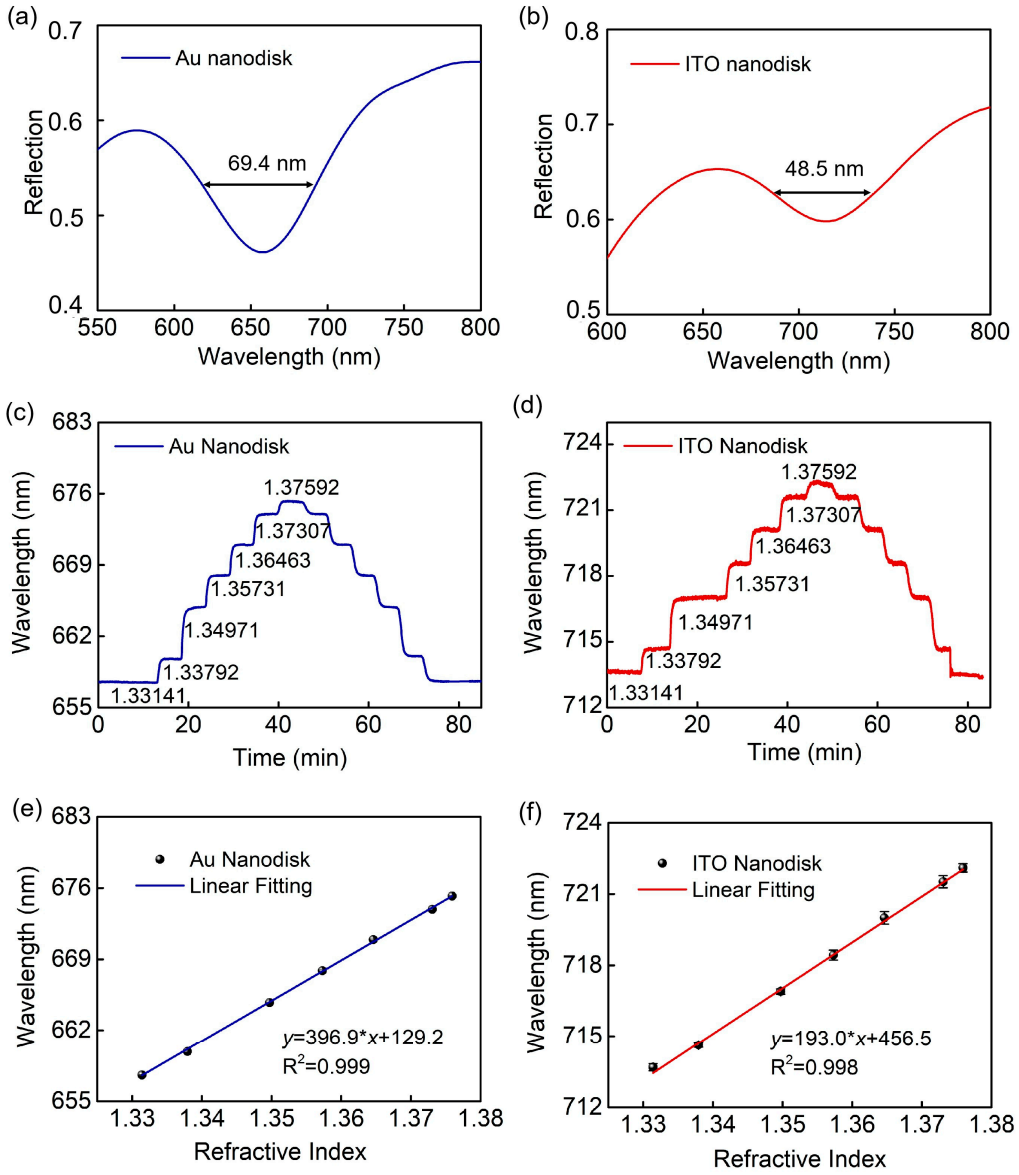

Figure 7. Measured dependence of resonance wavelength with refractive indices of different salt solution analytes. For all-metal nanodisk arrays, (a) typical spectrum in water, (c) temporal dependence, and (e) linear fitting of spectral positions. For ITO-Au nanodisk arrays, (b) typical spectrum in water, (d) temporal dependence, and (f) linear fitting of spectral positions.

To investigate the potential of the developed nanostructure for biosensing applications, we utilized plasmonic resonances for analyzing molecular binding events between immunoglobulin G (IgG) and anti-immunoglobulin G (anti-IgG). The specific surface modification process was categorized into two types. One pertained to the all-metal nanostructure array [27,28]. Initially, the sensor chip was immersed in a 10 mM solution of 11-mercaptoundecanoic acid (MUA) in ethanol for 12 hours to self-assemble a carboxylic layer, which was then dried with nitrogen. Later, an 1-(3-Dimethylaminopropyl)-3-ethylcarbodiimide hydro (EDC)/N-Hydroxy succinimide (NHS) mixed solution (0.5 M and 0.55 M) was used to activate hydroxyl groups on the nanostructure surface for 20 minutes at 4 ° C, and the surface was cleaned with deionized water. Subsequently, a 0.1 mg/mL anti-IgG phosphoric acid buffer solution (PBS, PH=7) was added to the surface for 30 minutes, followed by washing with PBS buffer. Lastly, the surface was coated with a 1 mg/mL of BSA solution for 15 minutes to prevent unmodified anti-IgG. With these steps, surface functionalization was complete. Human immunoglobulin IgG samples of 0.02, 0.1, 1.0, and 1.5 mg/mL were injected, and with an

Preprints (www.preprints.org) | NOT PEER-REVIEWED | Posted: 10 May 2023 doi:10.20944/preprints202305.0721.v1

increase in concentration, the resonance wavelength red-shifted. Through calculation and fitting, it was deduced that the equilibrium dissociation constant and the maximum wavelength shift were 120 μg/mL and 1.40 nm, respectively (Figure 8a).

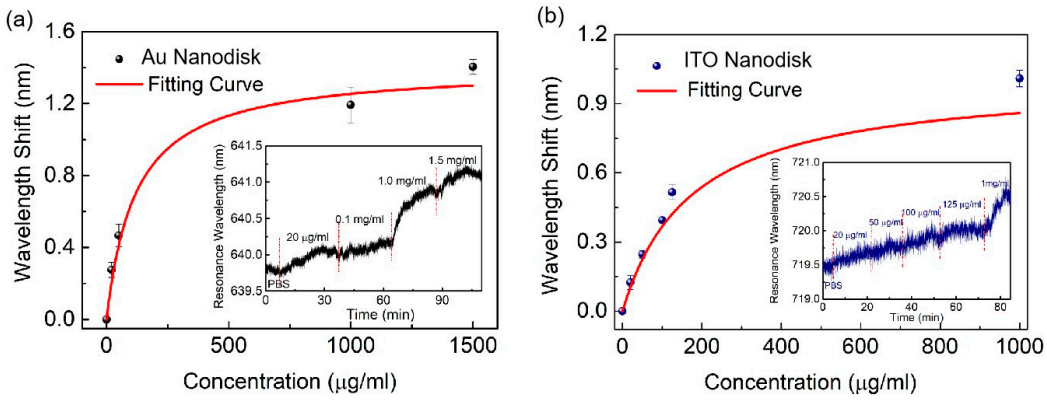

Figure 8. Probing of IgG with the resonance modes for the two nanostructures. (a) Full-metal nanodisk arrays. (b) ITO-Au nanodisk arrays.

The method mentioned above is applicable to thiol modification interactions with gold material, but not with ITO material. Therefore, in order to test the ITO-Au nanodisk arrays of IgG proteins, we utilized positive and negative charge adsorption. The IgG displays positive charge with a PH<6.9, while negative charge with a PH>6.9 [29,30]. In addition, PDDA was utilized as a strong cationic polyelectrolyte layer. The detection process involves immersing the sensor chip in a 1% mass fraction of PDDA solution for 15 minutes and then cleaning the surface with deionized water. We then immobilized anti-IgG with 1mg/mL onto the sensor surface using electrostatic adsorption for 30 minutes, followed by cleaning with PBS solution. Finally, termination processing was done by using BSA solution. IgG samples with different concentrations were detected. Similarly, the resonance wavelength shifts red as the concentration increases for ITO nanostructures. Through calculation and fitting, the equilibrium dissociation constant and the maximum wavelength shift are 180 μg/mL and 1.00 nm, respectively (Figure 8b). The results indicate that biosensing can be achieved through plasmonic full-metal nanodisk arrays and ITO-Au nanodisk arrays, which helps optimizes sensing performance and enriches the detection system.

3. Conclusions

In this paper, we developed a coupling mechanism that generated by ITO nanodisks on an Au substrate. This method effectively decreases the bandwidth and improves the sensing FOM when compared to full-metal nanostructures. The interaction between the ITO nanodisks and the Au substrate produces both SPP mode and magnetic resonance, leading into an ultra-narrow bandwidth for coupling resonance mode. We have demonstrated the biosensing application of this ITO-Au nanodisk arrays through specific antigen-antibody binding, with a detection limit of 180 μg/mL. This scheme provides a feasible option for coupling hybrid mechanisms, as well as potential promising biosensing performance.

Author Contributions: Author Contributions: Conceptualization, and software, S.C.; validation, S.C., Y.L. and M.L.; formal analysis, Y.L. and Y.H.; methodology, S.C. and Y.H.; investigation, S.C. and H.Y.; data curation, S.C., Y.L., H.Y. and J. M.; writing—original draft preparation, S.C.; writing—review and editing, W.P.; visualization, M.L. and J. M.; supervision, M.L., Y.L. and W.P.; project administration, W.P.; funding acquisition, W.P.; Resources, W.P.; All authors have read and agreed to the published version of the manuscript.

Funding: This work was supported by the National Natural Science Foundation of China (NSFC) (62171076, 12274052, 62105052, 6200031659), Fundamental Research Funds for the Central Universities (DUT20RC(3)008).

Data Availability Statement: Not applicable.

Conflicts of Interest: The authors declare no conflict of interest.

References

1. Gu, Y.; Zhang, L.; Yang, J. K.; Yeo S. P.; Qiu, C. W. Color generation via subwavelength plasmonic nanostructures. *Nanoscale*, **2015**, 7(15), 6409-6419.
2. Yang, W.; Xiao, S.; Song, Q.; Liu, Y.; Wu, Y.; Wang, S.; Yu, J.; Han, J.; Tsai, D. P. All-dielectric metasurface for high-performance structural color. *Nat. Commun.*, **2020**, 11(1), 1864.
3. Yao, Y.; Liao, Z. F.; Liu, Z. Q.; Liu, X. S.; Zhou, J.; Liu, G. Q.; Yi, Z.; Wang, J. Q. Recent progresses on metamaterials for optical absorption and sensing: a review. *J. Phys. D: Appl. Phys.*, **2021**, 54(11), 113002.
4. Yu, P.; Besteiro, L. V.; Huang, Y. J.; Wu, J.; Fu, L.; Tan, H. H.; Jagadish, C.; Wiederrecht, G. P.; Govorov, A. O.; Wang, Z. M. Broadband metamaterial absorbers. Adv. *Optical Mater.*, **2018**, 7(3), 1800995.
5. Nie, J.; Yu, J.; Liu, W.; Yu, T.; Gao, P. Ultra-narrowband perfect absorption of monolayer two-dimensional materials enabled by all-dielectric subwavelength gratings. *Opt. Express*, **2020**, 28(26), 38592-38602.
6. Bi, W.; Zhang, X.; Yan, M.; Zhao, L.; Ning, T.; Huo, Y. Low-threshold and controllable nanolaser based on quasi-BIC supported by an all-dielectric eccentric nanoring structure. *Opt. Express*, **2021**, 29(8), 12634-12643.
7. Zhu, W.; Xu, T.; Wang, H.; Zhang, C.; Deotare, P. B.; Agrawal, A.; Lezec, H. J. Surface plasmon polariton laser based on a metallic trench Fabry-Perot resonator. *Sci. Adv.*, **2017**, 3(10), 2375-2548.
8. Minopoli, A.; Acunzo, A.; Della, V. B.; Velotta, R. Nanostructured surfaces as plasmonic biosensors: a review. *Adv. Mater. Interfaces*, **2021**, 9(2), 2101133.
9. Mauriz, E.; Lechuga, L. M. Plasmonic biosensors for single-molecule biomedical analysis. *Biosensors*, **2021**, 11(4), 123.
10. Sharma, A. K.; Pandey, A. K. Self-referenced plasmonic sensor with TiO_2 grating on thin Au layer: simulated performance analysis in optical communication band. *J. Opt. Soc. Am. B*, **2019**, 36(8), F25-F31.
11. Akiyoshi, K.; Tanaka, Y. Y.; Ishida, T.; Shimura, T.; Tatsuma, T. Plasmonic-diffractive hybrid sensors based on a gold nanoprism array. *ACS Appl. Nano Mater.*, **2018**, 1(11), 5994-5999.
12. Ameen, A.; Hackett, L. P.; Seo, S.; Dar, F. K.; Gartia, M. R.; Goddard, L. L.; Liu, G. L. Plasmonic sensing of oncoproteins without resonance shift using 3D periodic nanocavity in nanocup arrays. *Adv. Opt. Mater.*, **2017**, 5(11), 1601051.
13. Kuo, C. W.; Wang, S. H.; Lo, S. C.; Yong, W. H.; Ho, Y. L.; Delaunay, J. J.; Tsai, W. S.; Wei, P. K. Sensitive Oligonucleotide Detection Using Resonant Coupling between Fano Resonance and Image Dipoles of Gold Nanoparticles. *ACS Appl. Mater. Interfaces*, **2022**, 14(12), 14012-14024.
14. Zhang, Y. H.; Liang, Z. Z.; Meng, D. J.; Qin, Z.; Fan, Y. D.; Shi, X. Y.; Smith, D. R.; Hou, E. Z. All-dielectric refractive index sensor based on Fano resonance with high sensitivity in the mid-infrared region. *Results Phys.*, **2021**, 24, 104129.
15. Wang, B. Q.; Yu, P.; Wang, W. H.; Zhang, X. T.; Kuo, H. C.; Xu, H. X.; Wang, Z. M. High-Q Plasmonic Resonances: Fundamentals and Applications. *Adv. Optical Mater.*, **2021**, 9(7), 2001520.
16. Kasani, S.; Curtin, K.; Wu, N. A review of 2D and 3D plasmonic nanostructure array patterns: fabrication, light management and sensing applications. *Nanophotonics*, **2019**, 8(12), 2065-2089.
17. Yang, K.; Yao, X.; Liu, B.; Ren, B. Metallic plasmonic array structures: principles, fabrications, properties, and applications. *Adv. Mater.*, **2021**, 33(50), e2007988.
18. Liang, Y.; Cui, W.; Li, L.; Yu, Z.; Peng, W.; Xu, T. Large-scale plasmonic nanodisk structures for a high sensitivity biosensing platform fabricated by transfer nanoprinting. *Adv. Optical Mater.*, **2019**, 7(7), 1801269.
19. Liu, B.; Chen, S.; Zhang, J.; Yao, X.; Zhong, J. h.; Lin, H. X.; Huang, T. X.; Yang, Z. L.; Zhu, J. F.; Liu, S.; Lienau, C.; Wang, L.; Ren, B. A Plasmonic Sensor Array with Ultrahigh Figures of Merit and Resonance Linewidths down to 3 nm. *Adv. Mater.*, **2018**, 30(12), 1706031.
20. Lu, X.; Zhang, L.; Zhang, T. Nanoslit-microcavity-based narrow band absorber for sensing applications. *Opt. Express*, **2015**, 23(16), 20715-20720.
21. Liu, H.; Zheng, L.; Ma, P.; Zhong, Y.; Liu, B.; Chen, X.; Liu, H. Metasurface generated polarization insensitive Fano resonance for high-performance refractive index sensing. *Opt. Express*, **2019**, 27(9), 13252-13262.
22. Chen, J.; Peng, C.; Qi, S. B.; Zhang, Q.; Tang, C. J.; Shen, X. Y.; Da, H. X.; Wang, L. H.; Park, G. S. Photonic microcavity-enhanced magnetic plasmon resonance of metamaterials for sensing applications. *IEEE Photon. Technol. Lett.*, **2019**, 31(2), 113-116.
23. Chu, S. W.; Liang, Y. Z.; Yuan, H. Z.; Yu, L.; Liu, Q.; Peng, W. Ultranarrow linewidth coupling resonance in flexible plasmonic nanopillar array for enhanced biomolecule detection. *Adv. Mater. Interfaces*, **2022**, 9(27), 8.
24. Hong, Q.; Luo, J.; Wen, C. C.; Zhang, J. F.; Zhu, Z. H.; Qin, S. Q.; Yuan, X. D.; Hybrid metal-graphene plasmonic sensor for multi-spectral sensing in both near- and mid-infrared ranges. *Opt. Express*, **2019**, 27(24), 35914-35924.
25. Vala, M.; Ertsgaard, C. T.; Wittenberg, N. J.; Oh S. H. Plasmonic sensing on symmetric nanohole arrays supporting high-Q hybrid modes and reflection geometry. *ACS Sens.*, **2019**, 4, 3265-3274.
26. Spackova B., Wrobel P., Bockova M., Homola, J. Optical biosensors Based on plasmonic nanostructures: a review. *Proc. IEEE*, **2016**, 104(12), 2380-2408.

 doi:10.20944/preprints202305.0721.v1

27. Conteduca, D.; Barth, I.; Pitruzzello, G.; Reardon, C. P.; Martins, E. R.; Krauss, T. F. Dielectric nanohole array metasurface for high-resolution near-field sensing and imaging. *Nat. Commun.*, **2021**, 12(1), 3293.
28. Yesilkoy, F.; Arvelo, E. R.; Jahani, Y.; Liu, M. K.; Tittl, A.; Cevher, V.; Kivshar, Y.; Altug, H. Ultrasensitive hyperspectral imaging and biodetection enabled by dielectric metasurfaces. *Nat. Photonics*, **2019**, 13(6), 390-396.
29. Caruso, F.; Niikura, K.; Furlong, D. N.; Okahata, Y. 2. Assembly of alternating polyelectrolyte and protein multilayer films for immunosensing. *Langmuir*, **1997**, 13(13), 3427-3433.
30. Wang, G. L.; Shu, J. X.; Dong, Y. M.; Xu, X. M.; Li, Z. J. An ultrasensitive and universal photoelectrochemical immunoassay based on enzyme mimetics enhanced signal amplification. *Biosens. Bioelectron*, **2015**, 66, 283-289.